

Synthesis, characterization and photocatalytic activity of PVP stabilized ZnO and modified ZnO nanostructures

Gauri Bandekar · N. S. Rajurkar · I. S. Mulla ·
U. P. Mulik · D. P. Amalnerkar · P. V. Adhyapak

Received: 8 June 2012 / Accepted: 26 December 2012 / Published online: 11 January 2013
© The Author(s) 2013. This article is published with open access at Springerlink.com

Abstract In the present study, ZnO nanostructures have been successfully synthesized by hydrothermal, sonochemical and precipitation methods using polyvinyl pyrrolidone (PVP) as the capping agent. The ZnO nanoparticles were characterized by X-ray diffraction (XRD), field emission scanning electron microscopy (FESEM), UV–Visible spectroscopy and photoluminescence (PL) techniques. The XRD results revealed the hexagonal wurtzite structure of the ZnO nanostructures for all the samples. Furthermore, the morphology of the ZnO particles was obtained from FESEM micrographs. Particles prepared by hydrothermal method were found to be rice grain shaped and that prepared by precipitation and sonochemical methods were spherical shaped. Sunlight driven photocatalytic degradation of methylene blue (MB) was studied for ZnO nanostructures synthesized by various methods. The ZnO nanostructures were further decorated with Ag nanoparticles to enhance its dye degradation efficiency. The Ag decorated ZnO nanoparticles exhibited a higher degradation rate as compared to pure ZnO nanoparticles which was independent of pH. Since this process of dye degradation relies on the degradation of dye due to oxidation by highly reactive hydroxyl radicals, there are many factors which affect the efficiency of this

process. Hence a study was conducted on the effect of various parameters on ZnO viz amount of catalyst, reaction pH and concentration of MB dye.

Keywords ZnO · Chemical precipitation · Hydrothermal · Sonochemical · Photocatalysis · Methylene blue

Introduction

The dyes are extensively used in textile, paper printing, food processing, cosmetics, pharmaceutical and leather industries. In recent years, environmental pollution due to the release of toxic chemicals from industrial sectors has been a major concern. Out of the 450,000 tons of organic dyes annually produced worldwide, more than 11 % find its way in effluents during manufacture and application processes (Forgas et al. 2004). This toxic effluent causes various environmental and health hazards (Parsons 2004). To overcome this issue researchers are working on various dye removal methods such as biodegradation, coagulation, adsorption, membrane process and advanced oxidation processes (AOPs). Among these processes the AOP is a balance process which includes widely studied sunlight driven photocatalysis process for removal of dyes. In this process electrons (in conduction band) and holes (in valence band) are generated using light energy. These holes and electrons interact with H₂O and O₂, respectively, to yield OH and OOH radicals (Behnajady et al. 2007; Akyol and Bayramoglu 2008; Anandan et al. 2007). These hydroxyl radicals are highly reactive with very high oxidation potential and can oxidize the dyes completely. It is a fast, clean and destructive method of dye degradation in which no secondary waste is generated (Fernandez et al. 2010).

G. Bandekar · N. S. Rajurkar
Department of Environmental Science, University of Pune,
Ganeshkhind, Pune 411007, India

N. S. Rajurkar
Department of Chemistry, University of Pune, Ganeshkhind,
Pune 411007, India

I. S. Mulla · U. P. Mulik · D. P. Amalnerkar ·
P. V. Adhyapak (✉)
Centre for Materials for Electronics Technology (C-MET),
Panchawati off Pashan Road, Pune 411008, India
e-mail: adhyapakp@yahoo.com; adhyapak@cmet.gov.in

Zinc oxide (ZnO) is one of the n-type semiconductors extensively used for AOP due to its wide band gap (3.3 eV) and large exciton binding energy (60 meV). It is also abundant in nature and is environmental friendly (Wahab et al. 2011). Moreover, ZnO is a better semiconductor as compared to commonly used TiO₂, because widespread use of TiO₂ has been proved to be uneconomical for large scale water treatment operations (Sobana and Swaminathan 2007). Nevertheless, ZnO can also effectively degrade dyes in acidic or basic medium, and is cheaper than TiO₂ (Yang et al. 2010; Xie and Wu 2010). The utmost advantage of ZnO is that it absorbs more light quanta in the UV spectrum as compared to TiO₂ (Behnajady et al. 2006).

Uptill now, a variety of methods have been developed for the synthesis of ZnO nanostructures which include hydrolysis in polyol medium (Poul et al. 2001), template method (Kou et al. 2006), chemical precipitation method (Wang et al. 2007a, b), thermal oxidation process (Zhang et al. 2007), hydrothermal (Zhou et al. 2007) and microwave synthesis (Siddiquey et al. 2008). These synthetic methods subsequently affect the morphology, size, crystalline form and photocatalytic activity of ZnO nanostructures (Zhang et al. 2007; Shi et al. 2004; Mohajerani et al. 2008). Therefore, ZnO nanostructures with diverse morphologies like nanowire (Huang et al. 2001), nanobelt (Pan et al. 2001), ellipsoidal (Liu et al. 2006; Xie et al. 2006; Pu et al. 2007), flower like (Tanner and Yu 2008), tube like (Yu et al. 2005) have been successfully synthesized. Effects of morphology and particle size on the photocatalytic activity of ZnO have also been studied and reported in the literature (Wang et al. 2007a, b; Jing et al. 2005; Dodd et al. 2006). For example, Jing et al. studied ZnO nanoparticles with three different sizes (14, 19, 26 nm) prepared by precipitation process. High surface oxygen vacancies, higher ESR intensity, stronger PL signal, and higher photocatalytic activity was observed for the smaller sized ZnO nanoparticles (Jing et al. 2005). Dodd et al. (2006) reported the synthesis of ZnO nanoparticles within 28–57 nm range by mechanical milling and heat treatment with maximum photocatalytic activity for 33 nm sized ZnO particle. Li et al. (2005) also obtained ZnO nanoparticles with average sizes 21–90 nm by varying the calcinations temperature between 200 and 1,000 °C and found that prismatic aggregated obtained by calcination at 800 °C demonstrated the highest photocatalytic activity. More recently, Wang et al. (2007a, b) showed that photocatalytic properties of various particle sizes of ZnO (15, 50, 200 and 1,000 nm) synthesized by thermal evaporation and chemical deposition in UV-induced degradation of methyl orange depended on size, morphology and preparation method of ZnO. Thus, according to previous reports, it is observed that the efficiency of photocatalytic process can

be maximized by optimizing the particle size, shape and preparation conditions/methods of ZnO photocatalysts.

We herein report, synthesis of ZnO nanostructures using three different methods viz hydrothermal, precipitation and sonochemical in presence of polyvinyl pyrrolidone (PVP) as a capping agent. The effect of synthetic methodology on the morphology and size of the nanostructures was studied. The sunlight driven photocatalytic activity of synthesized ZnO nanostructures was demonstrated using methylene blue (MB) as a representative dye. These ZnO nanostructures were further decorated with silver nanoparticles to enhance its photocatalytic activity. The degradation process is optimized with respect to catalyst dose, dye concentration and pH. The higher photocatalytic activity was achieved for ZnO with rice grain shape morphology obtained from hydrothermal process. To the best of our knowledge the photocatalytic activity is significantly higher than the other reports.

Experimental

Synthesis of nanostructured ZnO photocatalyst

All the chemicals used in this study were of analytical grade and used without further purification. Deionised water was used in all the experiments.

Three different synthetic schemes were used in the present study as follows:

Hydrothermal synthesis

Zinc acetate (CH₃COO)₂ Zn·2H₂O (6 g) and PVP (5 g) were dissolved separately in 15 mL methanol. These two solutions were mixed and were poured in a 250 mL Teflon vessel. A solution of NaOH was made by dissolving NaOH (6 g) pellets in 30 mL methanol. This NaOH solution was then slowly added to the above solution in Teflon vessel. A white precipitate was formed. Further, 5 mL of distilled water was added to this solution. The Teflon vessel was sealed and placed in a stainless steel autoclave. This stainless steel autoclave was placed in an oven at 70 °C for 24 h. The resultant precipitate was centrifuged and washed several times with distilled water and finally with acetone to remove the excess capping of PVP. After sufficient washings, the residue was dried at 70 °C for 24 h and ground to form a fine powder (Sample code ZN:1).

Precipitation method

Zinc acetate (6 g) and PVP (5 g) were separately dissolved in 30 mL methanol. The above mixture was mixed and kept on magnetic stirrer for constant mixing for 1 h. NaOH

solution was added dropwise to the above mixture and ZnO was allowed to precipitate completely. The above reaction mixture was covered and kept aside for aging for 24 h. The obtained white coloured precipitate was separated by centrifugation at 4,000 rpm and washed several times with distilled water till it was free from metal salts and finally with acetone. The residue was further dried at 70 °C for 24 h and then ground to form homogeneous powder (Sample code ZN:2).

Sonochemical method

Zinc acetate (6 g) and PVP (5 g) were dissolved separately in 15 mL methanol. These two solutions were admixed and kept for sonication for 15 min using probe sonicator (Sonics Vibra cell). After 15 min, NaOH solution was added dropwise to the above solution with continuous sonication. The white coloured precipitate occurred. This reaction mixture was further continued to sonicate for 45 min and kept aside for overnight aging. After 24 h, the milky suspension was centrifuged at 4,000 rpm for 10 min. The obtained white precipitate was washed several times with distilled water and finally with acetone. The residue was dried at 70 °C in oven and ground using motor and pestle to form final oxide powder (Sample code ZN:3).

Preparation of Ag decorated ZnO nanostructures

The ZnO nanoparticles synthesized by above three methods were further decorated with Ag nanoparticles. For this purpose, 2 wt % Ag loading was done for all ZnO samples. The detailed procedure is as follows: 0.5 g ZnO powder was suspended in freshly prepared 100 mL solution of 0.001 M AgNO₃ in a round bottom flask. The round bottom flask was sealed with a rubber cork and kept for constant stirring on a magnetic stirrer. After an hour few drops of dilute hydrazine hydrate were added to this solution. The colour of the solution turns violet. The resultant Ag decorated powder was separated by centrifuging the solution at 4,000 rpm. The powder was washed twice with distilled water and final washing of acetone was given to remove all the impurities (Sample code ZND:1, ZND:2 and ZND: 3 for hydrothermal, precipitation and sonochemical methods, respectively).

Physicochemical characterization

The physico-chemical characterization of pristine ZnO and Ag decorated ZnO nanoparticles was done by X-ray diffraction (XRD, Bruker D8-Advance X-Ray powder diffractometer) using CuK α radiation ($\lambda = 1.54 \text{ \AA}$). The scanning range was $20^\circ < \theta < 80^\circ$, voltage = 40 kV and current 40 mA. The morphology and size of the ZnO

nanoparticles was determined by field emission scanning electron microscopy (FESEM, Hitachi S-4800 SEM). The absorption spectra of ZnO samples were obtained by UV–Visible spectrophotometer (Jasco V-570 UV–Visible spectrophotometer). Photoluminescence (PL) measurements were obtained from Hitachi F-2500 Fluorescence spectrophotometer.

Photocatalytic experiments

The photocatalytic activity of ZnO nanoparticles was evaluated by degradation of MB dye solution. All the experiments were carried out in presence of sunlight. 100 mL (10 mg/L) MB dye solution was taken in a conical flask. To this 50 mg of ZnO catalyst was added and was stirred in dark for 10 min to allow the physical adsorption of dye molecules on the catalyst surface. This experimental setup was then placed in sunlight under constant stirring. To study the effect of pH on degradation efficiency, the pH of the MB dye solution was systematically adjusted by adding 0.1 M HCl or NaOH. The pH value of the solutions was measured by Cyberscan 500 pH meter at room temperature.

The samples (~5 mL) were collected at regular intervals from the reaction mixture and centrifuged to remove the suspended catalyst. The concentration of MB dye was determined from the absorption spectra of all the MB dye degradation samples obtained by UV–Visible spectrophotometer at $\lambda_{\text{max}} = 665 \text{ nm}$. The percentage dye degradation was calculated using formula:

$$\text{Degradation} = (C_0 - C) / C_0 \times 100 \% \quad (1)$$

where, C_0 is the initial dye concentration; C is the dye concentration at time (t)

Results and discussion

Characterization

The XRD patterns of the ZnO photocatalyst synthesized by three different methods are shown in Fig. 1. These X-ray diffractograms were analyzed to obtain information about various crystalline aspects. All the samples exhibit similar XRD patterns. The major diffraction peaks observed at 2θ values = 31.9° , 34.4° , 36.2° , 47.5° , 56.7° , 62.7° , 68.1° , 68.8° correspond to (100), (002), (101), (102), (110), (103), (112), (201) reflection planes, respectively. These results are in accordance with the reported literature (JCPDS 36-1541) which implies the hexagonal wurtzite structure of ZnO. Furthermore, it can also be seen that the enhanced intensity of (101) peak is dominant over all other peaks confirming the formation of hexagonal wurtzite structure.

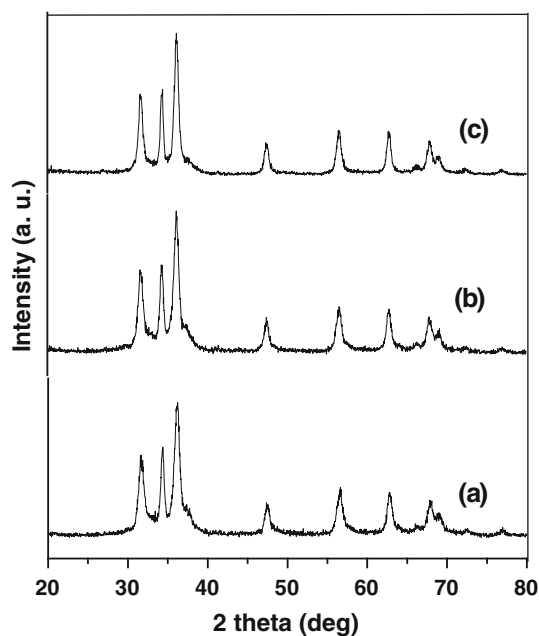


Fig. 1 XRD patterns of ZnO nanostructures synthesized by *a* hydrothermal, *b* precipitation and *c* sonochemical method

The sharp and intense peaks indicate that the samples are highly crystalline (Rekha et al. 2010). No any other impurity peaks were detected in diffraction patterns of ZnO obtained from three different methods indicating that the prepared photocatalysts were pure. The mean crystalline sizes of ZnO nanostructures were calculated using the Scherrer's formula:

$$D = 0.9\lambda / \beta \cos\theta \quad (2)$$

where λ is the wavelength of X-rays (1.540 for CuK α), θ is the Bragg's angle, β is the full width at half maximum. The calculated mean crystalline sizes of ZnO nanostructures synthesized by hydrothermal, precipitation and sonochemical method are 9.9, 9.3 and 8.6 nm, respectively.

Figure 2 displays the representative XRD pattern of Ag decorated ZnO sample obtained by hydrothermal method (sample ZND:1), in which there are three peaks at 38.1°, 44.2°, and 64.4° corresponding to (111), (200) and (220) planes of the Ag nanoparticles (Yin et al. 2012). It should also be noted that the peak of the (111) plane in intensity is comparatively intense than those of other two peaks, suggesting that the Ag NPs are mainly enclosed with the (111) planes. Furthermore, according to some previous reports, Ag can be incorporated in ZnO systems either as a substituent for Zn²⁺ or as an interstitial atom (Fan and Freer 1995; Blinks and Grimes 1993). If the silver is substituted for Zn²⁺, a corresponding shift would be expected in the XRD pattern. No such shift in the peak positions was observed in our modified sample, indicating the segregation

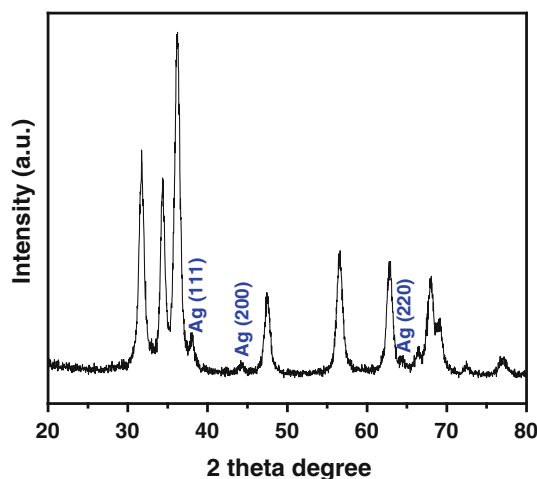


Fig. 2 Representative XRD pattern of Ag decorated rice grain shaped ZnO nanostructured sample: ZND:1

of Ag particles in the grain boundaries of ZnO crystallites rather than going into the lattice of ZnO.

Figure 3 displays FESEM photomicrographs of ZnO photocatalysts obtained from three different methods. Formation of rice grain type structure with mean diameter ~ 5 nm and length ~ 50 nm was observed in case of ZnO obtained from hydrothermal method (Fig. 3a, b). The products obtained by precipitation and sonochemical methods revealed spherical morphology (Fig. 3c–f). The average diameter of spheres is around 15–30 nm. It should be noted that irrespective of the synthetic methodologies all ZnO particles are uniform and homogeneously distributed.

It is well known that the optical absorption behaviour of photocatalyst could significantly affect the photocatalytic activity. Fig. 4 represents the optical absorption spectra of ZnO photocatalysts obtained from three different methods. Single absorption peak at ~ 360 – 370 nm was observed for all the samples. These results are similar to the results reported by Yang et al. (2010). The prepared ZnO samples showed good optical absorption behaviour, especially for UV light absorption. The band gap energy of ZnO nanostructures was calculated based on the absorption spectrum of the sample according to the equation

$$E_{bg} = 1,240 / \lambda \text{ (eV)} \quad (3)$$

where, E_{bg} is the band gap energy of the photocatalyst, λ is the wavelength in nm.

The calculated bandgap of the ZnO samples are 3.3, 3.4 and 3.4 eV for hydrothermal, precipitation and sonochemical methods, respectively. This indicates that synthesized ZnO has a suitable band gap for photocatalytic degradation of dyes. Furthermore, from UV–Vis spectra (Fig. 4), it is also observed that the optical absorption

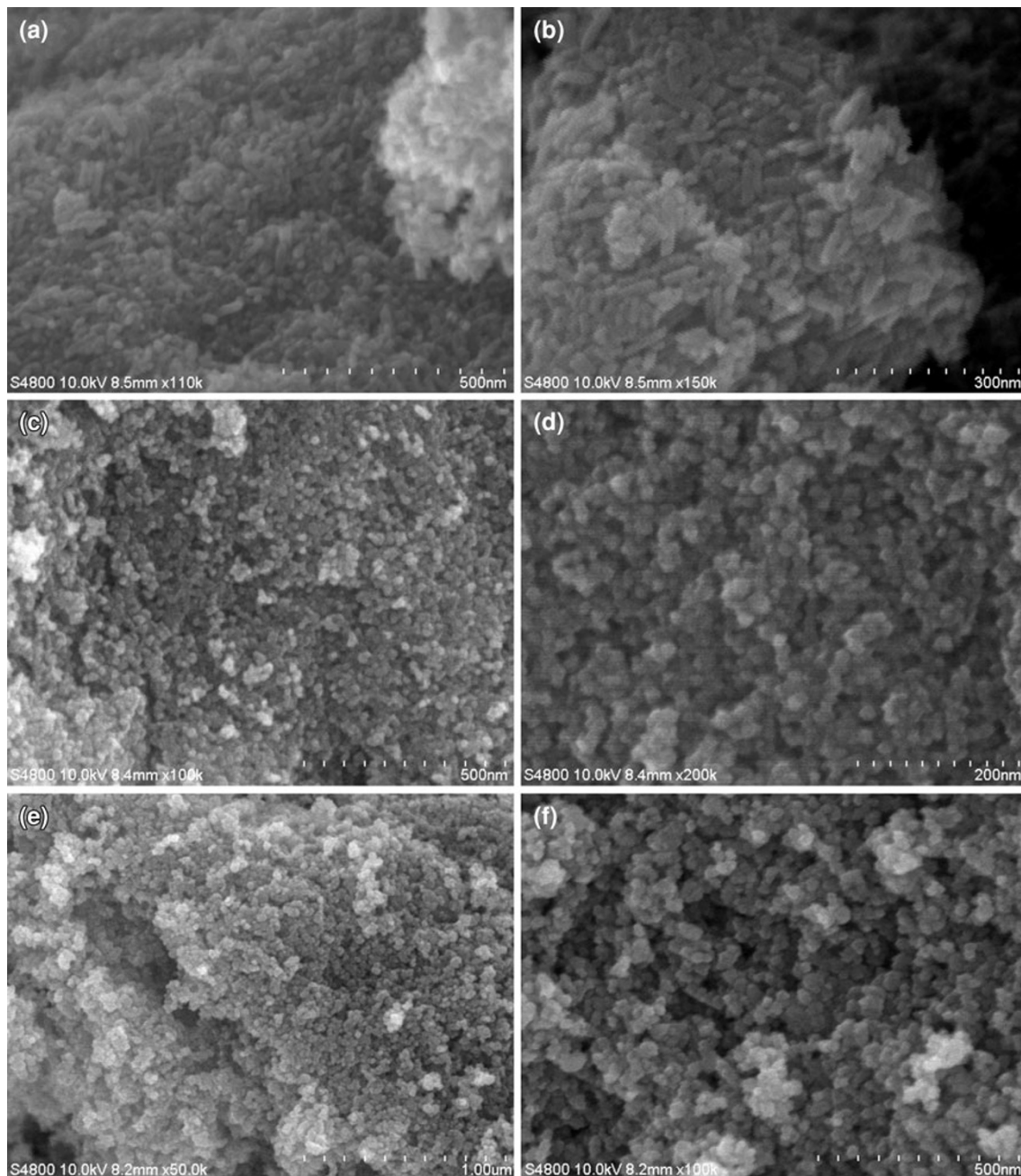


Fig. 3 Low and high magnification FESEM images of ZnO synthesized by (a, b) hydrothermal (c, d) precipitation and (e, f) sonochemical methods

behaviour is better in ZnO obtained from hydrothermal synthesis than the other two remaining samples.

The PL spectra are useful to disclose the efficiency of charge carrier trapping, immigration, and transfer and to understand the fate of electron hole pairs in semiconductor particles since PL emission results from the recombination of free carriers (Pawinrat et al. 2009). The PL spectra of ZnO photocatalysts were examined using 300 nm excitation wavelength and are depicted in Fig. 5. All the samples showed a strong emission peak ~ 380 nm (UV near band

edge) which can be attributed to the defect-related emissions and is in accordance with the reported values for ZnO, which possesses an exciton-related violet emission at 380 nm (Li et al. 2009).

Photocatalytic activity

The photodegradation of methylene blue was employed to evaluate the photocatalytic activities of the pristine and Ag decorated ZnO nanostructures. The photocatalytic

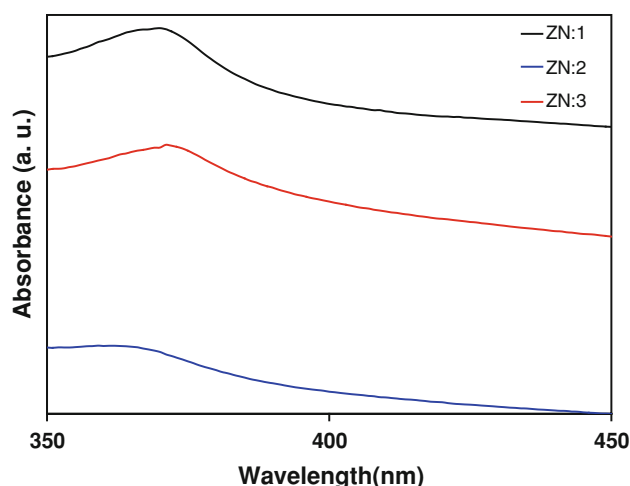


Fig. 4 Optical absorption spectra of ZnO synthesized by hydrothermal (ZN:1), precipitation (ZN:2) and sonochemical methods (ZN:3)

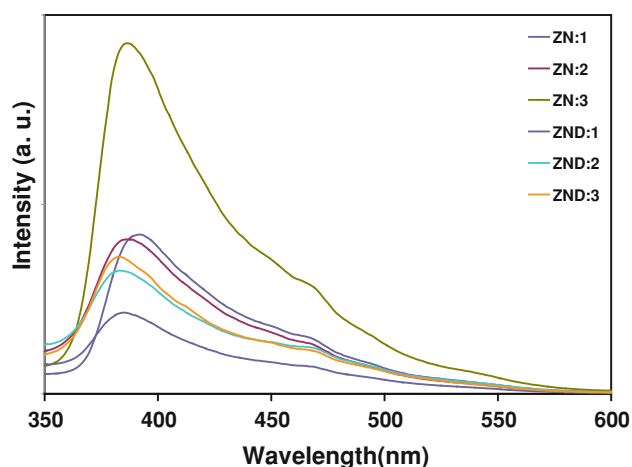


Fig. 5 Photoluminescence spectra of pure ZnO photocatalyst ZN:1, ZN:2 and ZN:3 and Ag decorated ZND:1, ZND:2 and ZND:3 synthesized by hydrothermal, precipitation and sonochemical methods, respectively at excitation wavelength of 300 nm

properties of ZnO are known to depend on several factors like size, morphology, surface area and electronic state. The self degradation of MB in UV light was negligible in the absence of photocatalyst.

Figure 6 presents the plot of $\ln(C_0/C)$ versus time, which clearly shows a linear relationship with the irradiation time, indicating that the photodegradation of the dye follows a pseudo first order kinetics. It is observed that the Ag decorated ZnO showed higher photodegradation efficiency as compared to pristine ZnO (Fig. 7). This is due to Ag decoration which provides active sites on the surface of ZnO and also reduces electron–hole recombination. The highest degradation activity was obtained for Ag decorated rice grain shaped ZnO nanoparticles. Many researchers have reported the effect of crystal size of ZnO on

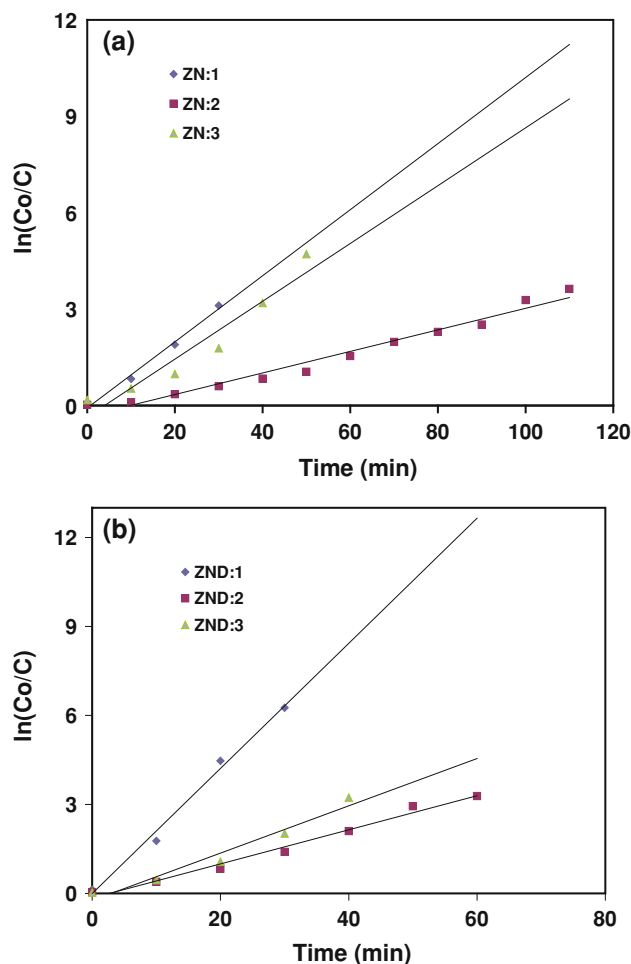


Fig. 6 Plots of $\ln C_0/C$ versus reaction time (min) for **a** pristine ZnO samples **b** Ag decorated ZnO samples obtained from different methods. Experimental conditions: [dye] = 10 mg L⁻¹, pH = 6.8, [ZnO] = 0.5 g L⁻¹

photocatalytic activity and also the optimum size for which photocatalytic activity is maximized. It is proved that when the particle sizes of nanostructures increase beyond the optimum size, the photocatalytic activity decreases due to decrease in surface area. The ZnO samples synthesized by hydrothermal method (ZN:1), precipitation method (ZN:2) and sonication method (ZN:3) took 45, 100 and 55 min, respectively for complete MB degradation. Recently, Lv et al. (2012) have reported a microwave-assisted synthesis of ZnO–reduced graphene oxide–carbon nanotube (CNT) composites and their application for MB dye degradation under UV irradiation. It was found that, the ZnO–RGO–CNT composite with 3.9 wt % CNTs achieves a maximum degradation efficiency of 96 % under UV light irradiation for 260 min of irradiation. Compared with these composites, our synthesized bare ZnO nanoparticles are having the enhanced photodegradation efficiency and advantage of operating under sunlight. Furthermore, Sun et al. (2012) have reported synthesis of nut-like, hexagonal

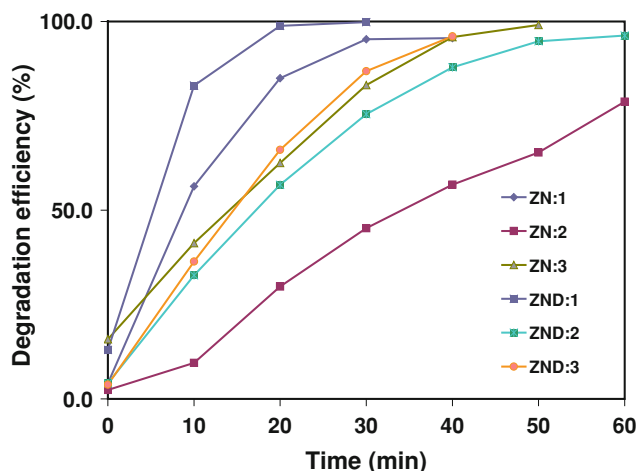


Fig. 7 Time profile of methylene blue degradation for pristine and Ag decorated ZnO nanostructures obtained from different methods

Table 1 Kinetic parameters data for degradation of MB by pristine and Ag decorated ZnO obtained from different methods

Sample code	Method	Kinetic equation	k (min^{-1})	R^2
ZN:1	Hydrothermal	$y = 1.027x - 1.101$	1.027	0.991
ZN:2	Precipitation	$y = 0.335x - 0.661$	0.335	0.972
ZN:3	Sonochemical	$y = 0.899x - 1.254$	0.899	0.925
ZND:1	Hydrothermal (Ag decorated)	$y = 2.109x - 2.115$	2.109	0.991
ZND:2	Precipitation (Ag decorated)	$y = 0.574x - 0.7373$	0.574	0.984
ZND:3	Sonochemical (Ag decorated)	$y = 0.797x - 1.031$	0.797	0.960

sphere-like, oblate-like and flower-like ZnO structures and studied the UV-assisted photodegradation of methylene blue dye. The results shows that, 100 mL, 10 mg/L of the aqueous MB dye solution was degraded after 180 min of UV light irradiation in presence of each of the studied photocatalyst (80 mg). In comparison with the above results, our synthesized ZnO nanostructures exhibit comparatively higher photocatalytic activity for degradation of MB dye. It can be seen from the Fig. 6a that ZN:1 sample has got the highest degradation efficiency with degradation rate constant $k = 1.027 \text{ min}^{-1}$ (Table 1).

The as-synthesized pristine ZnO nanostructures were modified by suspending ZnO powder in freshly prepared 0.001 M AgNO_3 solution. The major aim behind the modification of ZnO with Ag is to improve the catalytic property. The deposition of noble metals on semiconductor nanoparticles is an effective way for improving the photocatalytic efficiency, as the interfacial charge transfer processes are influenced by the metal modifier. As a noble metal silver can act as electron scavenger and store them

effectively. Light absorption of a suitable wavelength by ZnO results in the promotion of an electron from the valence band to the conduction band. The resulting hole is primarily responsible for the formation of hydroxyl radicals, which subsequently degrade the pollutants adsorbed onto the surface of catalyst. In such photocatalytic process, the separation and recombination of photogenerated charge carriers are competitive pathways and photocatalytic activity is effective when recombination between them is prevented. The extent of recombination can be estimated by the intensity of luminescence.

It can be seen from Fig. 5, that the UV emission of ZnO (centred at 380–390 nm) for Ag decorated ZnO reduces in the order ZND:1 > ZND:3 > ZND:2, respectively. This gradual decrease can be ascribed to the electron trapping effect of Ag, which acts as an electron acceptor species, hindering the recombination of charge carriers on ZnO. Accordingly, the superior photoactivity of ZND:1 ($2.109 \text{ k} [\text{min}^{-1}]$) followed by ZND:3 ($0.797 \text{ k} [\text{min}^{-1}]$) and ZND:1 ($0.574 \text{ k} [\text{min}^{-1}]$) was obtained in our case.

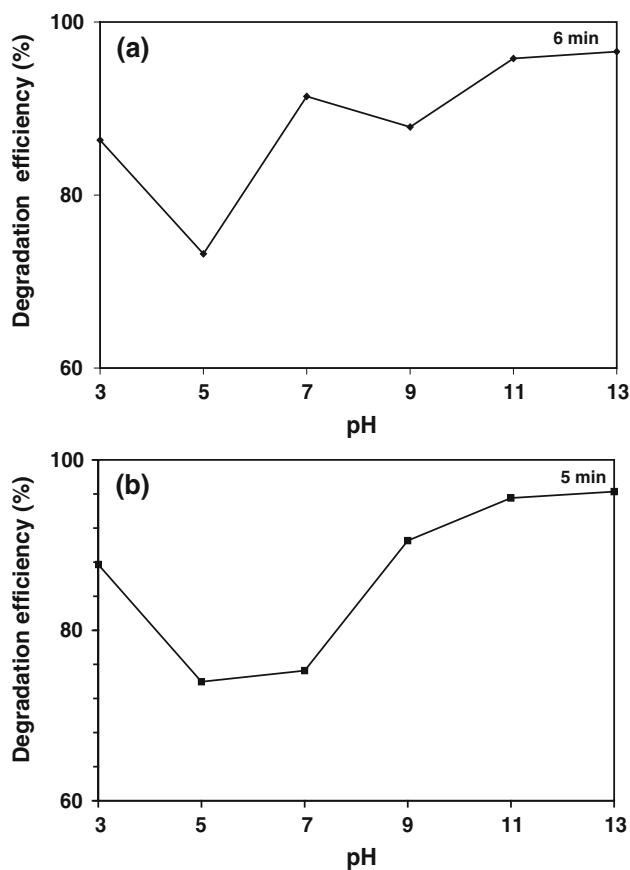


Fig. 8 Effect of pH on the photocatalytic activity of **a** rice shaped ZnO photocatalyst and **b** rice shaped Ag decorated ZnO photocatalyst. Experimental conditions: $[\text{dye}] = 10 \text{ mg L}^{-1}$, $[\text{ZnO}] = 0.5 \text{ g L}^{-1}$, reaction time = 15 min except for pH 13

Effect of pH

The effect of pH on the photocatalytic activity was studied by varying the pH of the dye solution. It can be seen from Fig. 8 that pH has a significant effect on the photodegradation rate. The rate of degradation increased with the increase in pH. There exists an electrostatic interaction between the catalyst surface and the dye molecules which consequently enhances or inhibits the photodegradation rate. The effect of pH value on photocatalysis is generally due to surface charge of the catalyst and the charge on dye molecules (Kong et al. 2010). The change in pH shifts the redox potentials of the valence and conduction bands, which might affect the interfacial charge transfer (Jiang et al. 2008; Chakrabarti et al. 2004). The surface of ZnO is positively charged at low pH whereas; with rise in pH the surface becomes negatively charged. As MB is a cationic dye, high pH favours the adsorption of dye molecule on the catalyst surface which results in high degradation efficiency. The degradation rate was found to

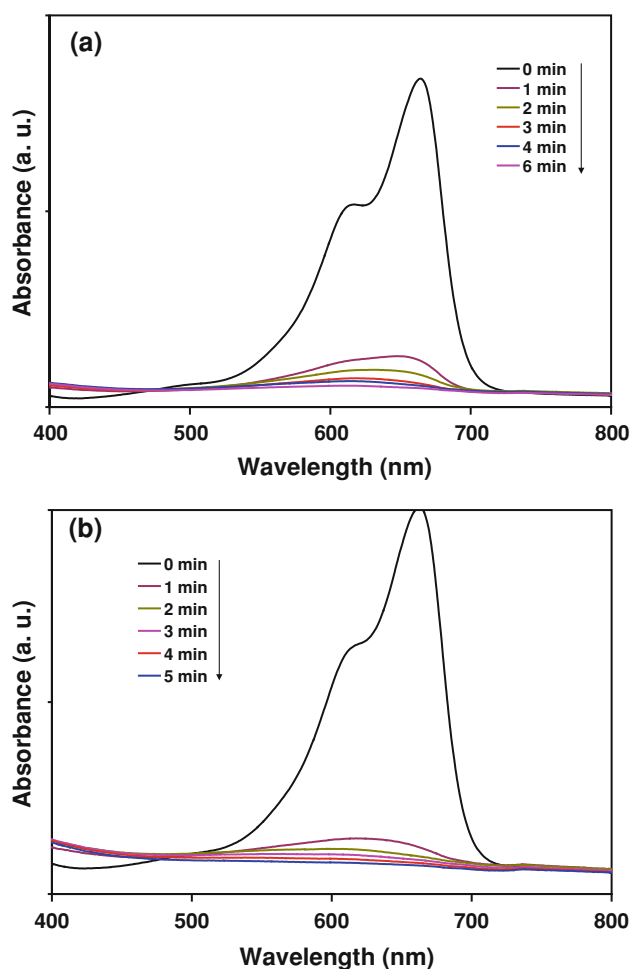


Fig. 9 UV-Visible spectra of photo-degradation reaction of methylene blue dye at pH-13 by **a** pure ZnO and **b** Ag decorated ZnO

be enhanced in alkaline conditions and maximum activity was obtained at pH 13. At pH 13, 96 % dye degradation is observed in 6 min for ZN:1 sample and 96 % dye degradation is observed in 5 min for ZND:1 sample (see Figs. 8, 9).

Effect of catalyst dose

The effect of catalyst dose on photo-degradation efficiency was studied by varying the catalyst dose. It is seen that the degradation efficiency of the MB increased with increase in the catalyst dose but after a certain concentration, the degradation efficiency decreases. This is due to impairment in light penetration with increasing catalyst dose. The increased catalyst dose increases the turbidity of the solution thus blocking the light and causing scattering. From Fig. 10, it can be seen that maximum photocatalytic degradation is seen at 50 mg dose of ZnO photocatalyst, as the dose was further increased the rate of degradation was affected.

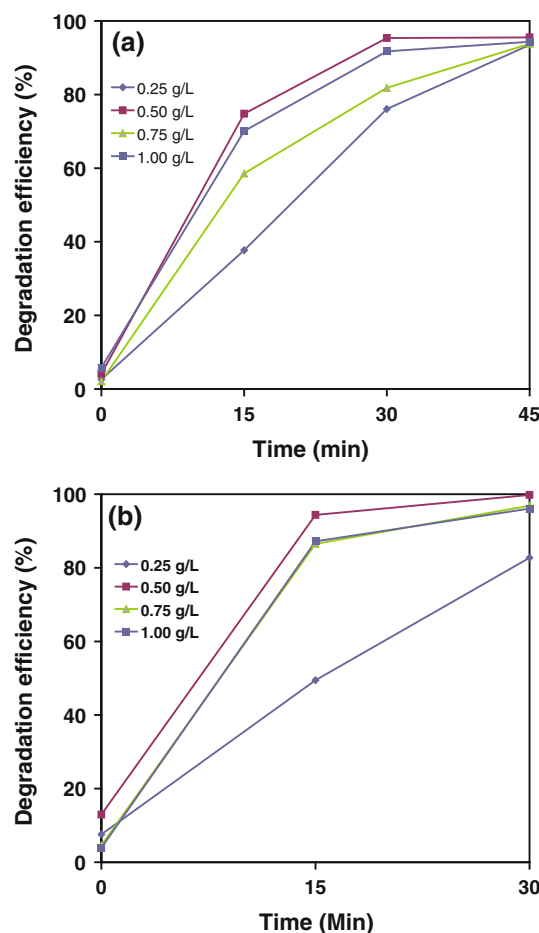


Fig. 10 Effect of catalyst dosage on the photocatalytic degradation of MB by rice shaped **a** pure ZnO **b** Ag decorated ZnO photocatalyst. Experimental conditions: [dye] = 10 mg L⁻¹, pH = 6.8

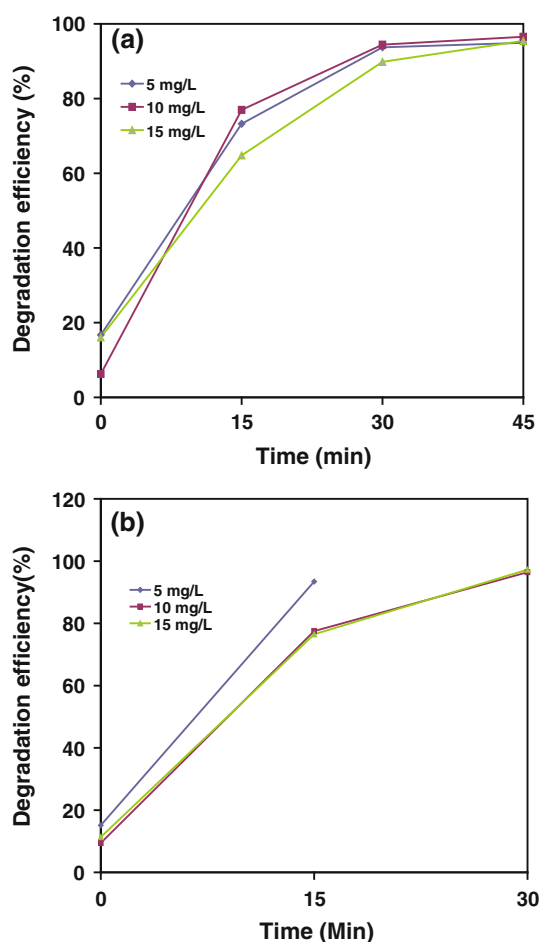


Fig. 11 Effect of initial dye concentration on the photocatalytic degradation of MB by the rice shaped **a** ZnO photocatalyst **b** Ag decorated ZnO. Experimental conditions: pH = 6.8, [ZnO] = 0.5 g L⁻¹

Effect of initial concentration of MB

The effect of initial concentration of MB on photocatalytic activity was studied by varying the initial dye concentration from 5–15 mg L⁻¹. The degradation efficiency is significantly dependent on the initial dye concentration; the results are shown in Fig. 11. The dye degradation efficiency decreases as the concentration of MB dye increased. This can be attributed to the number of hydroxyl radicals which remains constant as the ZnO catalyst dose was kept constant. Maximum dye degradation was observed at 5 mg L⁻¹ (Fig. 11). As the concentration of the dye increased the degradation efficiency decreased.

Conclusions

The present study outlines the synthesis of nanostructured ZnO photocatalyst by hydrothermal, precipitation and sonochemical methods using polyvinyl pyrrolidone as

capping agent. The physico-chemical characterization involved XRD, FESEM, UV–Visible and PL. The synthesized ZnO photocatalyst possessed hexagonal wurtzite structure. The unique rice grain shaped ZnO nanostructures were obtained from hydrothermal method. The photocatalytic activity of prepared ZnO photocatalyst was evaluated by methylene blue dye. The results clearly indicate that synthesized rice grain shaped ZnO photocatalyst shows higher photocatalytic activity as compared to ZnO synthesized by other two methods. Further Ag decoration of ZnO photocatalyst was done to enhance its degradation efficiency. The Ag decorated ZnO showed a higher degradation rate as compared to pristine ZnO photocatalyst independent of pH. The rate constant for Ag decorated ZnO photocatalyst is $k = 2.109$. It was found that degradation kinetics of MB fitted the pseudo first order kinetics. Furthermore, optimization of parameters was done for pristine and Ag decorated ZnO photocatalyst obtained by hydrothermal method. It was found that at pH 13; ~96 % dye degradation of MB is observed in 6 min for pristine sample and ~96 % dye degradation is observed in 5 min for Ag decorated sample. The above results show that the nanostructured ZnO photocatalyst exhibits excellent photocatalytic activity and can be considered as a promising photocatalyst for treatment of dye effluents.

Acknowledgments PVA thank Department of Electronics and Information Technology, New Delhi and ISM thank CSIR for Emeritus Scientist scheme.

Open Access This article is distributed under the terms of the Creative Commons Attribution License which permits any use, distribution, and reproduction in any medium, provided the original author(s) and the source are credited.

References

- Akyol A, Bayramoglu M (2008) The degradation of azo dye in a batch slurry photocatalytic reactor. *Chem Eng Proc* 47(12): 2150–2156
- Anandan S, Vinu A, Mori T, Gokulakrishna N, Shrinivasu P, Murugesan V, Ariga K (2007) Photocatalytic degradation of 2,4,6-trichlorophenol using lanthanum doped ZnO in aqueous suspension. *Catal Commun* 8(9):1377–1382
- Behnajady MA, Modirshahla N, Hamzavi R (2006) Kinetic study on photocatalytic degradation of CI acid yellow 23 by ZnO photocatalyst. *J Hazard Mater B* 133(1–3):226–232
- Behnajady MA, Modirshahla N, Daneshvar N, Rabbani M (2007) Photocatalytic degradation of CI acid red 27 by immobilised ZnO on glass plates in continuous mode. *J Hazard Mater* 140(1–2):257–263
- Blinks DJ, Grimes RW (1993) Incorporation of monovalent ions in ZnO and their influence on varistor degradation. *J Am Ceram Soc* 76(9):2370–2372
- Chakrabarti S, Dutta BK (2004) Photocatalytic degradation of model textile dyes in wastewater using ZnO as semiconductor catalyst. *J Hazard Mater* 112(3):269–278

- Dodd AC, Mckinley AJ, Saunders M, Tsuzuki T (2006) Effect of particle size on the photocatalyst activity of nanoparticulate ZnO. *J Nanopart Res* 8(1):43–51
- Fan J, Freer R (1995) The roles played by Ag and Al dopants in controlling the electrical properties of ZnO varistors. *J Appl Phys* 77(9):4750–4756
- Fernandez C, Larrechi MS, Pilar Callao M (2010) An analytical overview of processes for removing organic dyes from wastewater effluents. *Trends Anal Chem* 29(10):1202–1210
- Forgas E, Cserhati T, Oros G (2004) Removal of synthetic dyes from wastewater: a review. *Environ Int* 30(7):953–971
- Huang MH, Mao S, Feick H, Yan HQ, Wu YY, Kind H, Weber E, Russo R, Yang PD (2001) Room-temperature ultraviolet nanowire nanolasers. *Science* 292(5523):1897–1899
- Jiang YH, Sun YM, Liu H, Zhu FH, Yin HB (2008) Solar photocatalytic decolorization of C.I. Basic blue 41 in an aqueous suspension of TiO₂-ZnO. *Dyes Pigment* 78(1):77–83
- Jing L, Yuan F, Hou H, Xin B, Cai W, Fu H (2005) Relationships of surface oxygen vacancies with photoluminescence and photocatalytic performance of ZnO nanoparticles. *Sci China Ser B Chem* 48(1):25–30
- Kong JZ, Li AD, Li XY, Zhai HF, Zhang WQ, Gong YP, Li H, Wu D (2010) Photodegradation of methylene blue using Ta-doped ZnO nanoparticle. *J Solid State Chem* 183(6):1359–1364
- Kou HM, Wang J, Pan YB, Guo JK (2006) Fabrication of hollow ZnO microsphere with Zinc powder precursor. *Mater Chem Phys* 99(2–3):325–328
- Li D, Balek V, Ohashi N, Mitsunashi T, Hishita S, Haneda H (2005) Self assembly prismatic aggregates formed during the calcination of ZnO powders: in situ monitoring by ETA technique and their photocatalytic properties. *J Colloid Interface Sci* 289(2):472–478
- Li F, Bi W, Liu L, Li Z, Huang X (2009) Preparation and characterization of ZnO nanospindles and ZnO@ZnS core-shell microspindles. *Colloids Surf A* 334(1–3):160–164
- Liu JP, Huang XT, Sulieman KM, Sun FL, He X (2006) Solution-based growth and optical properties of self-assembled monocrySTALLINE ZnO ellipsoids. *J Phys Chem B* 110(22):10612–10618
- Lv T, Pan L, Liu X, Sun Z (2012) Enhanced photocatalytic degradation of methylene blue by ZnO—reduced graphene oxide—carbon nanotube composites synthesized via microwave-assisted reaction. *Catal Sci Technol* 2(11):2297–2301
- Mohajerani MS, Mazloumi M, Lak A, Kajbafvala A, Zanganeth S, Sadmezhad SK (2008) Self-assembled zinc oxide nanostructures via a rapid microwave-assisted route. *J Cryst Growth* 310(15):3621–3625
- Pan ZW, Dai ZR, Wang ZL (2001) Nanobelts of semiconducting oxides. *Science* 291(5510):1947–1949
- Parsons S (2004) Advanced oxidation processes for water and wastewater. IWA Publishing, London
- Pawinrat P, Mekasuwandumrong O, Panpranot J (2009) Synthesis of Au-ZnO and Pt-ZnO nanocomposites by one step flame spray pyrolysis and its application for photocatalytic degradation of dyes. *Catal Commun* 10(10):1380–1385
- Poul L, Ammar S, Jouini N, Fieovet F, Villain F (2001) Metastable solid solutions in the system ZnO-CoO: synthesis by hydrolysis in polyol medium and study of the morphological characteristics. *Solid State Sci* 3(1–2):31–42
- Pu XP, Zhang DF, Jia LP, Su CH (2007) Synthesis of zinc oxide nanostructures with controlled morphologies using a simple sonochemical method. *J Am Ceram Soc* 90(12):4076–4078
- Rekha K, Nirmala M, Manjula G, Anukaliani NA (2010) Structural, optical, photocatalytic and antibacterial activity of zinc oxide and manganese doped ZnO nanoparticles. *Physica B* 405(15):3180–3185
- Shi XY, Shen MW, Mohwald H (2004) Polyelectrolyte multilayer nanostructures toward the synthesis of diverse nanostructured materials. *Prog Polym Sci* 29(10):987–1019
- Siddiquey IA, Furusawa T, Sato M, Suzuki N (2008) Microwave-assisted silica coating and photocatalytic activities of ZnO nanoparticles. *Mater Res Bull* 43(12):3416–3424
- Sobana N, Swaminathan M (2007) Combination effect of ZnO and activated carbon for solar assisted photocatalytic degradation of Direct Blue 53. *Sol Energy Mater Sol Cells* 91(8):727–734
- Sun L, Shao R, Chen Z, Tang L, Dai L, Ding J (2012) Alkali-dependent synthesis of flower-like ZnO structures with enhanced photocatalytic activity via facile hydrothermal method. *Appl Surf Sci* 258(14):5455–5461
- Tanner PA, Yu LX (2008) Photoluminescence of ZnO:Eu³⁺ nano-flowers. *J Nanosci Nanotechnol* 8(3):1307–1311
- Wahab R, Hwang IH, Kim YS, Shin HS (2011) Photocatalytic activity of zinc oxide micro-flowers synthesized via solution method. *Chem Eng J* 168(1):359–366
- Wang H, Xie C, Zhang W, Cai S, Gui Y (2007a) Comparison of dye degradation efficiency using ZnO powders with various size scales. *J Hazard Mater* 141(3):645–652
- Wang SM, Yang ZS, Lu MK, Zhou YY, Zhou GJ, Qui ZF, Wang SF, Zhang HP, Zhang AY (2007b) Coprecipitation synthesis of hollow Zn₂SnO₄ spheres. *Mater Lett* 61(14–15):3005–3008
- Xie JS, Wu QS (2010) One-pot synthesis of ZnO/Ag nanospheres with enhanced photocatalytic activity. *Mater Lett* 64(3):389–392
- Xie RG, Li DS, Zhang H, Yang DR, Jiang MH, Sekiguchi T, Liu BD, Bando Y (2006) Low-temperature growth of uniform ZnO particles with controllable ellipsoidal morphologies and characteristic luminescence patterns. *J Phys Chem B* 110(39):19147–19153
- Yang LY, Dong SY, Sun JH, Feng JL, Wu QH, Sun SP (2010) Microwave-assisted preparation, characterization and photocatalytic properties of a dumbbell-shaped ZnO photocatalyst. *J Hazard Mater* 179(1–3):438–443
- Yin X, Que W, Fei D, Shen F, Guo Q (2012) Ag nanoparticle/ZnO nanorod nanocomposites derived by a seed-mediated method and their photocatalytic properties. *J Alloys Compd* 524:13–21
- Yu HD, Zhang ZP, Han MY, Hao XT, Zhu FR (2005) A general low-temperature route for large-scale fabrication of highly oriented ZnO nanorod/nanotube arrays. *J Am Chem Soc* 127(8):2378–2379
- Zhang Y, Zhang WF, Zheng HW (2007) Fabrication and photoluminescence properties of ZnO:Zn hollow microspheres. *Scripta Mater* 57(4):313–316
- Zhou H, Fan TX, Zhang D (2007) Hydrothermal synthesis of ZnO hollow spheres using spherobacterium as biotemplates. *Microporous Mesoporous Mater* 100(1–3):322–327